

## **Chapter 2**

# **Synthesis of Materials and Characterization**

### **2.1 Introduction**

In the study related to materials, there are two important aspects that are considered. First are the different synthesis methods that can be used for the preparation of the material and second aspect corresponds to the various characterization techniques that are utilized to study the properties of the synthesized material. This chapter discusses the synthesis procedure of the bulk powder samples that constitute the present study and the characterization techniques used, relevant to the study. The techniques employed in the present study for characterization involves X-ray Diffraction (XRD) for structural studies, Raman Spectroscopy to analyze the vibrational modes that give rise to Raman active peaks. The optical band gap of semiconducting material is inferred from the UV-Vis spectroscopy. However, for semiconductors having a very small value of band gap that falls outside the UV or Visible region, Fourier Transform Infrared Spectroscopy (FTIR) technique is adopted. Electrical properties of the materials are measured using Physical Property Measurement System (PPMS) in the presence of magnetic field. Superconducting Quantum Interferometer Device (SQUID) is used to perform DC magnetization as well as AC magnetization measurements to understand the magnetic interactions present in the system. A brief introduction of the synthesis mechanism and the experimental techniques used are discussed in the ensuing sections.

### **2.2 Preparation of Bulk Sample**

Preparation of sample is an important aspect in material research. While preparing the samples, utmost care must be taken to avoid any kind of contamination. For this reason, the purity of the starting elements must be as high

as possible. The preparation method adopted should be such that the sample can be easily reproduced thereby maintaining its phase and other properties. The method employed for the sample preparation in the present study is not only cost effective but also yields good quality bulk samples.

For the preparation of bulk alloys of  $\text{Fe}_{0.05}(\text{Te})_{1-x}\text{Sb}_x$ , where  $x = 0, 0.01, 0.03$  and  $0.05$ ,  $\text{Fe}_{0.05}(\text{SnSe})_{1-x}\text{Sb}_x$ , where  $x = 0, 0.03$  and  $0.05$ , and  $\text{Fe}_{0.05}(\text{SnTe})_{1-x}\text{Sb}_x$ , where  $x = 0, 0.01, 0.03$  and  $0.05$ , high purity powder samples of different elements and compounds (~99.999% Alfa Aesar, USA) are utilized. The bulk alloys are then prepared by modified solid state technique that involves vacuum sealing of quartz tube which is discussed in the subsequent section.

### **2.2.1 Modified Solid State Technique**

Bulk samples of transition metal doped Te, SnSe and SnTe alloys along with the substitution of group V, nonmagnetic element Antimony (Sb), are prepared by taking desirable quantities of the starting materials in quartz tube ampoules. These ampoules are then vacuum sealed after evacuating them with a pressure of  $>10^{-5}$  Torr. Further, the materials present in the ampoules are melted by exposing them to an oxy-butane flame. The process of melting is repeated several times by periodically cooling the ampoules to room temperature, until a homogeneity is attained. In the end, they are quenched in cold water and ingots of the final product are obtained. Vacuum sealing unit from Hind High Vacuum Company Pvt Ltd, as shown in Fig. 2.1, is used which consists of roughing, backing and rotary pumps to evacuate the air molecules from within the ampoules.



*Figure 2.1:* Vacuum sealing unit for evacuating the ampoules at pressure  $> 10^{-5}$  Torr.

## **2.3 Techniques used for characterization**

The different techniques used for characterization purposes help in understanding the underlying properties of the material. They form an essential part of material research. These properties aid us to explore their probabilities for practical applications. The characterization techniques used for the present study has been briefly introduced in the following sections.

### **2.3.1 X-Ray Diffraction (XRD)**

X-rays on interacting with a crystalline material gives a diffraction pattern which is a fingerprint of that particular material. It a powerful, non-destructive technique that helps in analyzing different crystal structures, determination of unit cell parameters, average crystallite size, amount of strain in the material, phase purity, etc. The peak intensity of diffraction pattern can help in realizing atomic distribution in various crystal planes. The reason X-rays are used for examining the crystalline structure is based on the fact that the wavelength of X-rays are proportionate to the atomic size. To produce X-rays, highly accelerated electron

beams, that is achieved using high voltage supply, is made to bombard on a metal target. The commonly used metal targets are Copper and Molybdenum. X-rays produced from Copper (Cu) have an energy of 8 keV and wavelength of 1.54 Å whereas that produced from Molybdenum (Mo) have an energy of 14 keV and wavelength of 0.8 Å. The  $K_{\alpha}$  radiation of Copper has wavelength in the intermediate range which helps in acquiring the diffraction pattern without compromising with the accuracy of d-spacing. On the other hand, Molybdenum being a heavy metal, is able to produce X-rays that has low penetrability and high intensity. The X-rays are then made to incident on the sample and from the atomic planes present in the crystalline structure, these rays are reflected at a particular characteristic angle. The reflected rays may undergo either constructive or destructive interference. Constructive interference of the reflected rays is responsible for the diffraction pattern that is obtained by scanning the sample at  $2\theta$  range of angles. Diagrams representing the components of XRD and the constructive interference are shown in Fig. 2.2 and Fig. 2.3 respectively.

X-ray diffraction pattern is governed by Bragg's law which is given by the equation

$$n\lambda = 2d\sin\theta \quad (2.1)$$

n is order of diffraction,  $\lambda$  is wavelength of X-ray beam, d is interplaner distance and  $\theta$  is angle of diffraction. Due to certain instrumental factors, we observe broadening of diffraction peaks. The width of the broadened peak is used to calculate average crystallite size using Scherrer's relation [1] given by the equation

$$D = \frac{0.9\lambda}{\beta\cos\theta} \quad (2.2)$$

where  $\beta$  is Full Width at Half Maximum (FWHM) of the diffracted peak. The literature has further information about X-ray diffraction [2, 3]. Bruker D8 Advance X-ray Diffractometer with  $\text{CuK}_\alpha$  radiation at UGC-DAE-CSR, Indore was used to record the diffraction pattern at room temperature in the present study. The samples were scanned in the  $2\theta$  range of  $20^\circ$  to  $70^\circ$  having a step size of  $0.02^\circ$  and a scanning rate of  $2^\circ/\text{minute}$ .

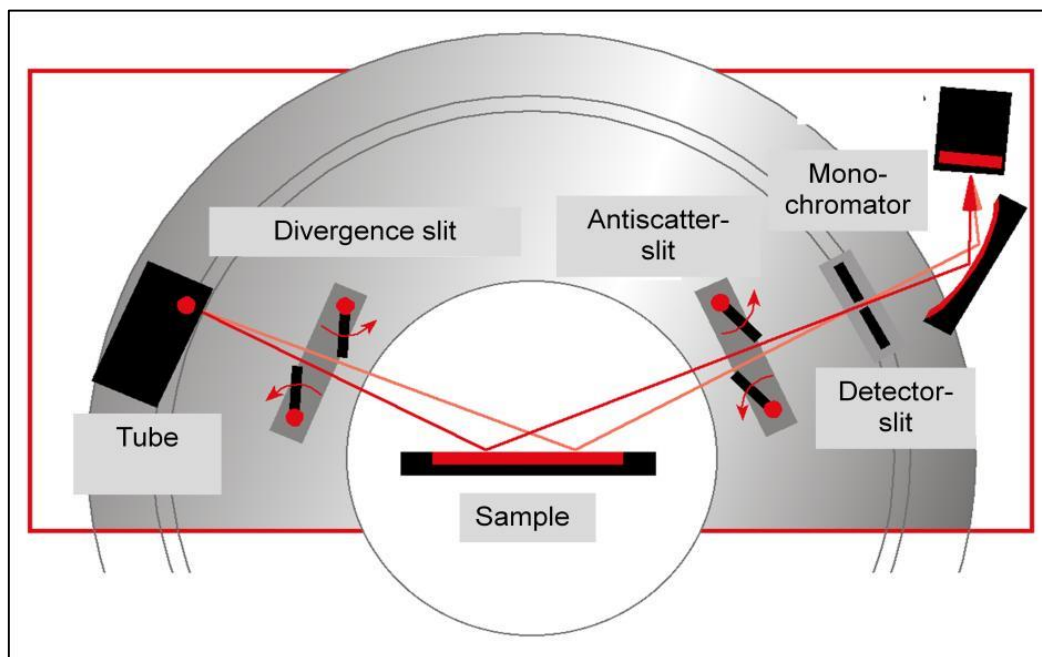


**Figure 2.2:** Representational diagram of X-ray diffractometer.

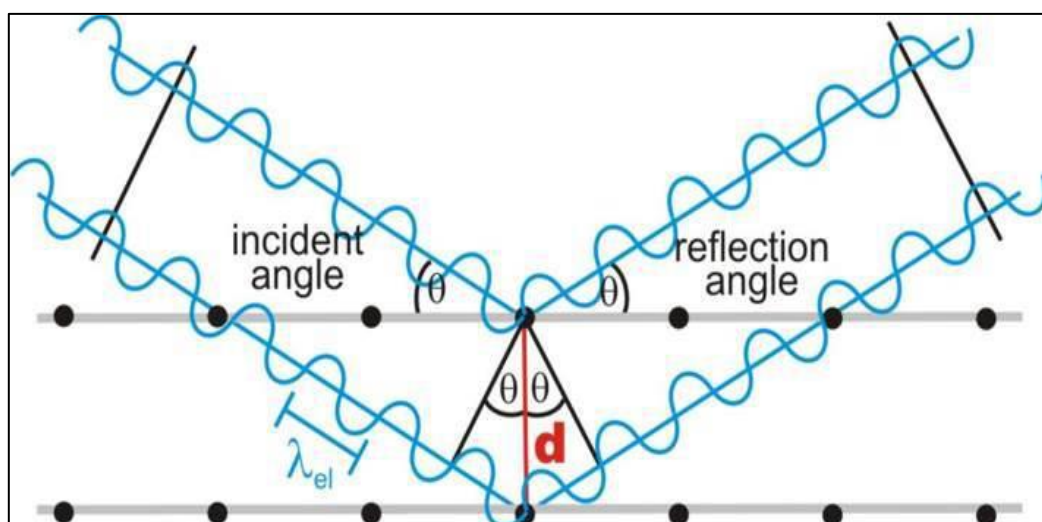


**Figure 2.3:** Diagram representing constructive interference of reflected rays.

### 2.3.2 Field Emission Scanning Electron Microscope (FESEM)

The main advantage of electron microscope over optical microscope lies in the fact that they use electron beam which gives it a higher resolution and higher range of magnification. A Scanning Electron Microscope (SEM) is mainly used to understand the topography, structure and also calculate the crystallite size of the sample under consideration. However, in comparison with Scanning Electron Microscope (SEM), Field Emission Scanning Electron Microscope (FESEM) is able to produce images that are much sharper and less electrostatically distorted [4]. Spatial resolution of an FESEM is down to few nanometers and a magnification from about 10 times to 3,00,000 times can be obtained. Fig. 2.4 is a representational diagram of Field Emission Scanning Electron Microscope. The main components of an FESEM are electron gun/Schottky field emitter, condenser lens, objective lens, scan coils and stigmator.

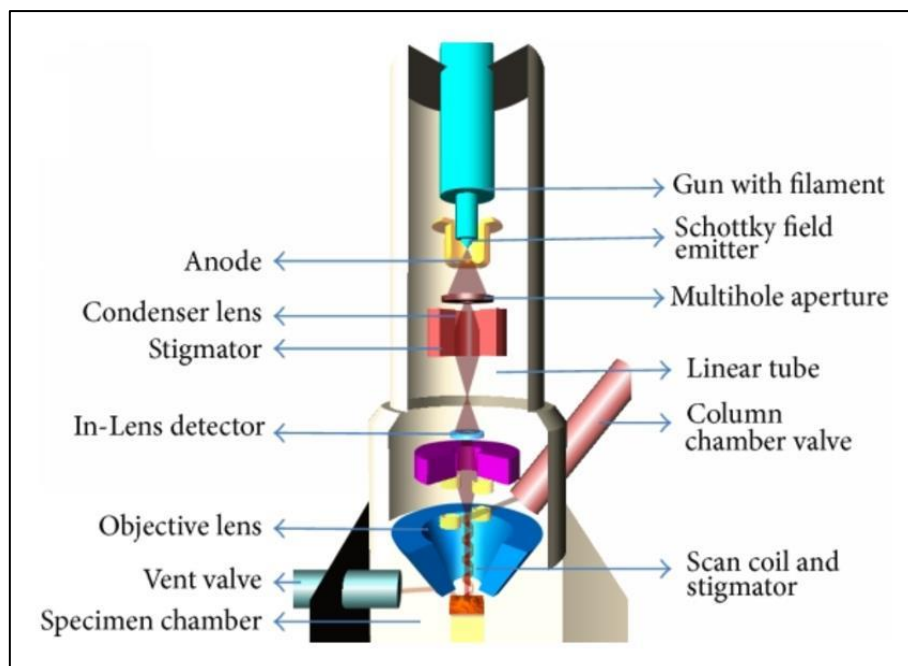


*Figure 2.4:* Representational diagram of Field Emission Scanning Electron Microscope (FESEM).

The electrons are generated from the Schottky field emitter gun and the electron beam is characterized by small diameter, high coherency and greater brightness. The beam of electrons are then passed through a combination of

apertures and lenses in order to obtain a focused beam of electrons in a vacuum evacuated chamber. These electrons are made to strike on the sample surface. Scanning coils control the position of electron beam striking the sample surface thereby enabling to scan the surface in a raster pattern. This provides information regarding a small area on the sample surface. Electrons on interacting with the sample produces secondary electrons, back-scattered electrons and characteristic X-rays. These electrons are then detected using suitable detectors to produce an image. The signals arising from secondary electrons and X-rays are produced due to interaction of primary electrons inside the sample. Secondary electrons have energies less than 50 eV whereas back-scattered electrons have energies greater than 50 eV [5]. The topography of the samples are observed using Field Emission Scanning electron microscope of Hitachi model S 3400 N.

### 2.3.3 UV-Vis Diffuse Reflectance Spectroscopy (DRS)

In order to find the optical band gap of a semiconducting material, UV-Vis Diffuse Reflectance Spectroscopy method is used. UV-Vis spectrum shows essentially no absorption for photons that have energies below the band gap and a significant absorption for photons above the band gap energy values. Apart from band gap energy, it can also provide details regarding the presence of different bonding's in the system. UV-Vis light is passed through the sample and the detector measures the intensity of light that is transmitted by the sample.

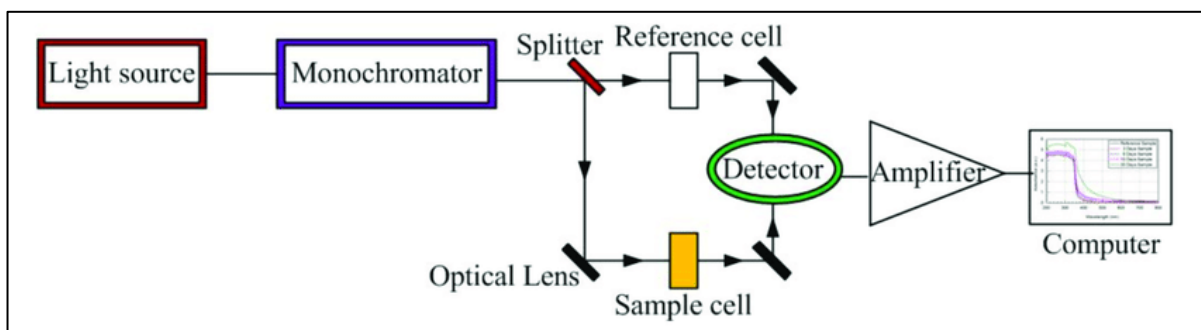


*Figure 2.5:* Representational diagram of UV-Vis spectrometer.

The set-up of UV-Vis spectrometer is shown in Fig. 2.5. UV-Vis spectrometer has two light sources, namely tungsten lamp that emits visible light and deuterium lamp that emits UV light. The visible and UV light then passes through slits into the monochromator, from which the output light obtained is a monochromatic in nature. This monochromatic beam of light is split into two beams of equal intensity by passing it through a set of mirrors. One beam passes through the reference and the other beam passes through the sample. The sample and reference are kept in a cuvette made up of either silica or quartz. Photodiode based detectors are used to record the beams coming from the sample and reference, and spectra is displayed on the computer attached to it.

Optical band gap of the sample is deduced from Tauc's relation expressed as

$$(\alpha h\nu)^{1/n} = B(h\nu - E_g) \quad (2.3)$$

where B is a proportionality constant,  $E_g$  is optical band gap and n depends on the type of transition i.e. n can take values 1/2, 2, 3/2 and 3 for direct allowed, indirect allowed, forbidden direct and forbidden indirect respectively [6].  $\alpha$  is the absorption coefficient which describes the rate at which the light intensity decreases along the path of its propagation. In reflectance mode, the reflected beam is measured by the spectrometer. Diffuse reflectance occurs when a fraction of the beam incident on the sample surface is reflected at various angles. To further increase the process of diffuse reflectance in samples, dilution of samples in non-absorbing matrix materials like KBr, KCl, etc was proposed by Kubelka and Munk [7]. According to the Kubelka – Munk theory, the measured reflectance can be converted into absorption co-efficient by making use of Kubelka – Munk radiative transfer model where

$$F(R) = \frac{(1-R)^2}{2R} = \frac{\alpha}{S} \quad (2.4)$$

F(R) is Kubelka – Munk function, R is reflectance,  $\alpha$  is absorption co-efficient and S is scattering co-efficient. F(R) will be equal to  $\alpha$  if scattering co-efficient S is not independent of wavelength. Substituting for  $\alpha$  as F(R) in equation (2.3), we can re-write it as

$$(F(R).hv)^{1/n} = B(hv - E_g) \quad (2.5)$$

In the present study, the UV-Vis spectra of the samples are recorded using Perkin Elmer Lambda 950 at UGC-DAE-CSR, Indore from 500 – 1500 nm range of wavelength.

#### **2.3.4 Fourier Transform Infrared Spectroscopy (FTIR)**

Fourier Transform Infrared Spectroscopy (FTIR) is a commonly used analytical technique to identify different functional groups, types of chemical bonds that are present in a sample. By recognizing the connection between an interferogram's spectrum and its Fourier transformation, Michelson and Lord Rayleigh set the groundwork for modern FTIR in the latter half of the nineteenth century [8, 9]. Absorption of infrared radiation results in a change in the vibrational as well as rotational energies of the molecules in the bonds. The infrared spectrum thus obtained is a molecular vibrational spectrum. Whether the vibration involves stretching, bending or twisting of bonds depends on the atoms present in the bond. In addition, exposing sample to infrared radiation results in selective absorption of specific frequencies which corresponds to their structure. This causes a change in the dipole moment of the sample molecules and such samples are known as IR-active [10]. Since different bonds and functional groups absorb different frequencies, the spectra obtained is fingerprint of a particular molecule under consideration. The spectra is recorded either in transmittance (%T) or absorbance (%A) mode as a function of wavenumber ( $\text{cm}^{-1}$ ).

The most important component of FTIR spectrometer is the Michelson Interferometer. Fig. 2.6 shows block diagram of FTIR spectrometer. IR radiation emitted from the IR source passes through the interferometer to the sample. The radiation is split by the beam splitter and the two beams go in direction at right angles to each other. One half of the beam reaches a fixed mirror and gets reflected back to the beam splitter. The other half goes to a moving mirror thereby creating a path difference. These two beams recombine at the beam splitter that creates either constructive or destructive interference. The sample receives this interfering beam, or interferogram, and the transmitted portion of the interferogram is relayed to a detector. The measured signal is sent to the computer where it is reconstructed using Fourier Transform technique. Eventually, a plot of either transmittance or absorbance as a function of wavenumber is obtained as an infrared spectrum.

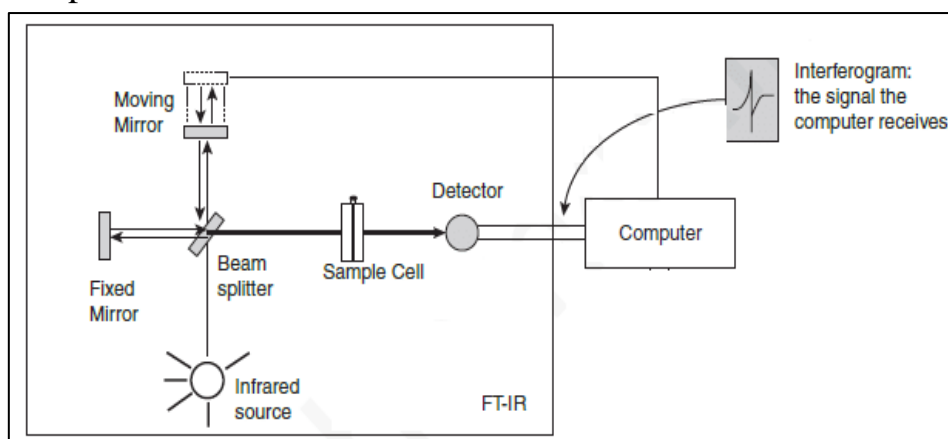


**Figure 2.6:** Block diagram of FTIR spectrometer.

The band gap of those semiconductors that is small enough to fall in the UV-Vis range can be deduced from the FTIR spectrum. In case of the samples that are studied, the transmittance spectra is converted into absorbance spectra using the relation

$$A = -\log_{10} \frac{1}{T} \quad (2.6)$$

Further, using Tauc's relation from equation (2.3), the band gap of the samples can be calculated considering similar conventions for the value of n. For the

present research work, FTIR spectrum of  $\text{Fe}_{0.05}(\text{SnTe})_{1-x}\text{Sb}_x$  ( $x = 0, 0.01, 0.03$  and  $0.05$ ) samples are recorded using Shimadzu FTIR – 8400 S at Department of Applied Chemistry, The Maharaja Sayajirao University of Baroda, Vadodara, whereas that of  $\text{Fe}_{0.05}(\text{Te})_{1-x}\text{Sb}_x$  ( $x = 0, 0.01, 0.03$  and  $0.05$ ) samples are recorded using Bruker Optics make ALPHA-T Spectrometer at Department of Chemistry, The Maharaja Sayajirao University of Baroda, Vadodara.

### 2.3.5 Raman Spectroscopy

Raman Spectroscopy is a versatile, spectroscopic technique that provides non-destructive analysis of the molecular structure by giving information regarding its vibrational, rotational and other low-frequency modes of molecules. A monochromatic beam of light, typically from a laser source, is incident upon the sample and a spectrometer detects the scattered light. The monochromatic light beam undergoes inelastic scattering due to which a change is observed in the frequency of incident photons. These photons are initially absorbed by the sample and then re-emitted. As a result, the re-emitted photons have their frequencies shifted, either up or down, in comparison to the original frequency of the incident light. This phenomenon is known as Raman Effect.

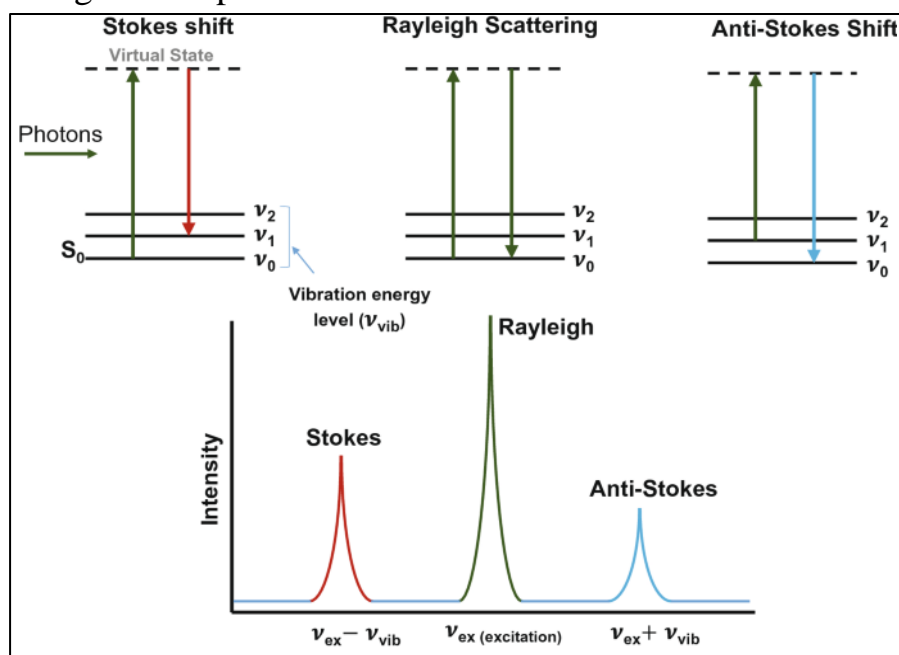


**Figure 2.7:** Schematic diagram showing Raman scattering from the energy level diagram and positions of the Raman peaks.

Raman effect occurs due to change in molecular polarizability ( $\alpha$ ) whereas IR spectra arises due to change in dipole moment of the molecule [11]. These techniques are considered complementary to each other. When a beam of monochromatic light is irradiated on the sample, a large portion of absorbed photons are scattered at the same frequency or wavelength as that of incident photons. This process is known as elastic scattering or Rayleigh scattering. The remaining photons that are absorbed undergo scattering that results in a shift in the frequency or wavelength. The shift towards lower frequency is known as Stokes shift whereas that towards the higher frequency is known as Anti-Stokes shift. The intensity of Anti-Stokes line is smaller than that of Stokes line. Figure 2.7 represents the Raman effect diagrammatically. Thus, in Raman spectroscopy, it is the intensity of Stokes line that is recorded as a function of change in frequency with respect to the incident radiation, in units of wavenumber ( $\text{cm}^{-1}$ ). Raman activity is influenced by both space group and point group symmetry of a crystalline solid and that of a molecule respectively. The symmetry of the crystal is, however, contained in its crystallographic point group [12].

Early Raman spectrometers used mercury arc lamps which is now replaced by laser light as they provide intense beam of radiation that are highly monochromatic in nature. A combination of notch filter and grating monochromator is used to isolate a single laser beam and minimize Rayleigh scattering. The scattered photons that correspond to Raman peaks are detected using charge-coupled device (CCD) detectors. The representational diagram of Raman spectrometer is shown in Fig. 2.8. Raman scattering studies of the samples are performed using Raman spectrometer of micro-Raman model STR 500 with Nd-YAG laser source of 532 nm wavelength and Peltier cooled CCD detector equipped with Nikon microscope of different objective lenses at Department of Physics, The Maharaja Sayajirao University of Baroda, Vadodara.

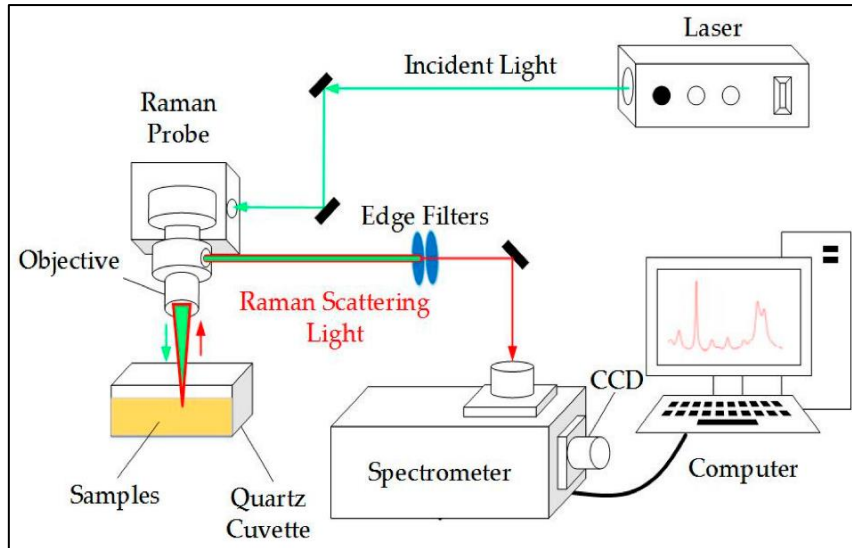


*Figure 2.8:* Representational diagram of Raman spectrometer.

### 2.3.6 Physical Property Measurement System (PPMS)

Electrical properties of semiconducting materials are investigated by carrying out DC resistivity measurements. They help in gaining an insight into the charge transportation properties. The resistivity of a material is given by

$$\rho = \frac{R \times T \times W}{l} \quad (2.7)$$

Since powder samples cannot be directly utilized for DC resistivity studies, they are pressed under pelletizer to form rectangular pellets. The dimensions of the pellet are represented by W (width), T (thickness), l (distance) between the 2 metallic contacts and R, the measured resistance giving Eq. 7. Through resistivity measurements, we can study the magneto transport properties of samples which will give information regarding different types of interactions like electron-electron interaction, electron-magnon interaction, electron-phonon interaction, electron-electron and electron-phonon scattering [13, 14].

Physical Property Measurement System (PPMS) is designed to measure a variety of physical properties of the sample while controlling the conditions experienced by the sample. It is used to perform automated electrical and magnetic measurements. Resistivity measurements at temperatures as low as 2 K

and magnetic field up to 14 T can be carried out. The cross-sectional representation of PPMS system is shown in Fig. 2.9. To determine resistivity, electrical contacts are made on the material using either two probe method or four probe method [15]. Under four probe method, the two commonly used mechanisms are four-point collinear probe method and van der Pauw method [16, 17].

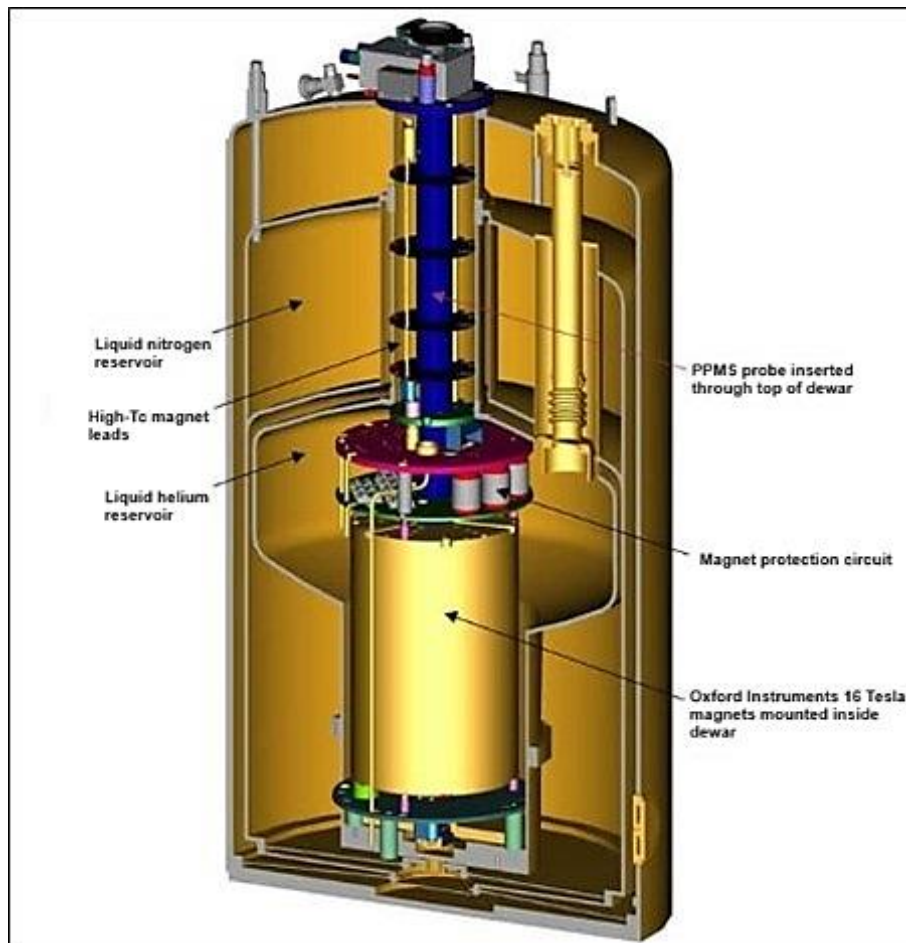


**Figure 2.9:** Internal cross-section structure of PPMS system.

The different techniques to determine the resistivity of the material varies depending on the type of the material, magnitude of resistance and the dimensions of the material. Two probe method is suitable for those samples which has high resistivity, whereas for low resistivity samples, four probe method serves better. This is because there are separate leads for current and voltage in four probe method. Also, the contact and spreading resistances of the probes in four probe

method are quite low compared to that of two probe method. Fig. 2.10 shows puck holder for resistivity measurement in the PPMS system. The pellet is stuck onto the insulating paper and contacts are made (two for current and two for voltage) on the sample surface. Quantum Design make Physical Property Measurement System at UGC-DAE-CSR, Indore is utilized in the present work for resistivity (R-T) and magnetoresistance (R-H) measurements of the samples.



*Figure 2.10:* Physical Property Measurement System in UGC-DAE-CSR, Indore.

### **2.3.7 Super Conducting Quantum Interface Device – Vibrating Sample magnetometer (SQUID - VSM)**

SQUID – VSM magnetometer is the most sensitive sensor to study the magnetic properties of materials. Samples that have weak magnetic moment can be detected easily using this instrument. The phenomena governing the functioning of the magnetometer are superconductivity, Josephson effect and magnetic flux quantization [18]. It consists of two superconductors which are separated by thin insulating layers that results in two parallel Josephson junctions. Such superconductors experience Cooper pair electron tunneling through the junction [19].

SQUID – VSM uses a superconducting magnet (a solenoid of superconducting wire) so that samples are subjected to magnetic fields of up to 7 Tesla. Liquid helium is used to cool not only the SQUID and magnet but also the sample chamber, thereby controlling the temperature of samples from 300 K to 2 K. Not only liquid helium but liquid nitrogen is also essential for proper functioning of the magnetometer. SQUID – VSM utilizes analytic techniques employed by vibrating sample magnetometers (VSM). The magnetized specimen is moved up and down through flux transformers, which are superconducting pick-up coils outside the sample chamber. The sample motion causes a change in magnetic flux resulting in a current to flow within the pick-up coils. This current, then carried to the SQUID input coil through the superconducting wires, is directly proportional to magnetic flux changes produced by the sample. The schematic of SQUID – VSM is shown in Fig. 2.11.

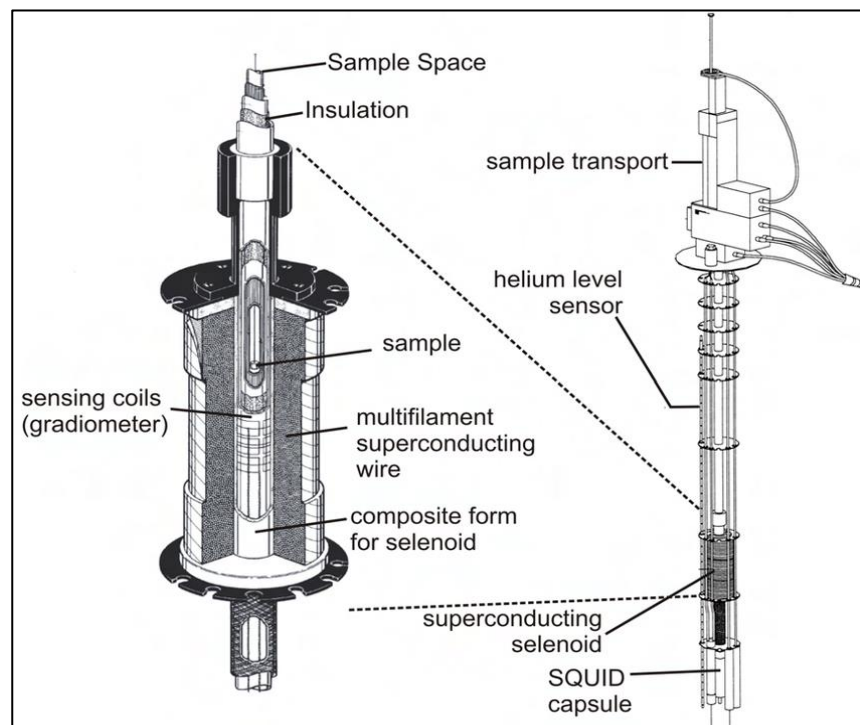


*Figure 2.11:* Schematic representation of SQUID-VSM device.

Both AC and DC magnetization measurements are possible through the SQUID – VSM magnetometer. However, the AC and DC magnetometers have different operational methods. DC magnetometer consists of a superconducting

ring having two Josephson junctions whereas AC magnetometer has only one Josephson junction [20]. For the present work, DC magnetization measurements of M-T under zero-field cooled (ZFC) and field cooled (FC) conditions as well as M-H at different temperatures are carried out using Quantum design make SQUID – VSM magnetometer system equipped with a pulse tube cooler at CIF, IISER, Bhopal. AC susceptibility measurement at different frequencies is also performed using the instrument. Magnetic memory effect measurement of some samples are also carried out at CRF, IIT Kharagpur by adopting the procedure as suggested by Sun et al. [21]. The samples are cooled by exposing them to an external magnetic field which is accompanied with intermittent stops at specified temperatures for a fixed duration of time wherein the magnetic field is switched off. After reaching the lowest temperature, the samples are then warmed continuously again in the presence of magnetic field. Magnetization data is recorded under both conditions to examine the memory retaining capability of the samples.

## References

1. P. Scherrer, "Gottinger Nachrichten," vol. 2, 98 (1918).
2. M. J. Buerger, "X-ray Crsytallography," John Wiley & Sons, New York (1942).
3. B. D. Cullity, "Elements of X-Ray diffraction," Addison-Wesley Publishing, Massachusetts (1956).
4. A. Mayeen, L. K. Shaji, A. K. Nair and N. Kalarikkal, "Morphological Characterization of Nanomaterials: Characterization of Nanomaterials," Woodhead Publishing, 335 (2018).
5. I. M. Watt, "The Principles and Practice of Electron Microscopy," Cambridge University Press, New York (1997).
6. F. P. Koffyberg, K. Dwight and A. Wold, "Interband transitions of semiconducting oxides determined from photoelectrolysis spectra," Solid State Communications, vol. 30, 433 (1979).
7. P. Kubelka and F. Munk, "A contribution to the optics of pigments," Z. Tech. Phys., vol. 12, 593 (1931).
8. A. A. Michelson, "Visibility of interference-fringes in the focus of a telescope," Phil. Mag., vol. 31, 256 (1891).
9. D. K. Schroder, "Semiconductor material and device characterization," John Wiley & Sons, New York (1990).
10. H. W. Siesler, Y. Ozaki, S. Kawata, and H. M. Heise, "Near-infrared spectroscopy: principles, instruments, applications," John Wiley & Sons, Weinheim, Germany (2008).
11. C.V. Raman and K.S. Krishnan, "The production of new radiations by light scattering," Proc. Roy. Soc. London, vol. A122, 23 (1929).

12. M. R. Derrick, D. Stulik and J. M. Landry, "Infrared Spectroscopy in Conservation Science," The Getty Conservation Institute, Los Angeles (1999).
13. G. J. Snyder, R. Hiskers, S. DiCarolis, M. R. Beasley, T. H. Geballe, "Intrinsic electrical transport and magnetic properties of  $\text{La}_{0.67}\text{Ca}_{0.33}\text{MnO}_3$  and  $\text{La}_{0.67}\text{Sr}_{0.33}\text{MnO}_3$  MOCVD thin films and bulk material," *Phys. Rev. B*, vol. 53, 14434 (1996).
14. R. Skini, M. Khlifi, M. Wali, E. Dhahri, E. K. Hlil and P. Lachkar, "Electrical transport and giant magnetoresistance in  $\text{La}_{0.8-x}\text{Ca}_{0.2}\text{MnO}_3$  ( $x=0, 0.1$  and  $0.2$ ) oxides," *J. Magn. Magn. Mater.*, vol. 363, 217 (2014).
15. D. K. Schroder, "Semiconductor material and device characterization," John Wiley & Sons, New York (1998).
16. L. J. van der Pauw, "A method of measuring the resistivity and hall coefficient on lamellae of arbitrary shape," *Philips Tech. Rev.*, vol. 20, 220 (1958/1959).
17. R. A. Witte, "Electronic Test Instruments (Analog and Digital Measurements)," Prentice Hall, New Jersey (2002).
18. F. London, "Superfluids: Macroscopic theory of superconductivity," vol. 1, John Wiley & Sons, New York (1950).
19. B. D. Josephson, "Possible new effects in superconductive tunneling," *Physics Letters*, vol. 1, 251 (1962).
20. R. L. Fagaly, "Superconducting quantum interference device instruments and applications," *Rev. Sci. Instrum.*, vol. 77, 101101 (2006).

21. Y. Sun, M. B. Salamon, K. Garnier and R. S. Averback, “Memory Effects in an Interacting Magnetic Nanoparticle System,” *Phys. Rev. Lett.*, vol. 91, 167206 (2003).